Atmospheric
Measurement
Techniques

Ground-based remote sensing scheme for monitoring aerosol–cloud interactions

Karolina Sarna and Herman W. J. Russchenberg

TU Delft Climate Institute, Faculty of Civil Engineering and Geotechnology, Delft University of Technology,
Stevinweg 1, 2628 CN, Delft, the Netherlands

Correspondence to: Karolina Sarna (k.sarna@tudelft.nl)

Abstract. A new method for continuous observation of aerosol–cloud interactions with ground-based remote sensing instruments is presented. The main goal of this method is to enable the monitoring of the change of the cloud droplet size due to the change in the aerosol concentration. We use high-resolution measurements from a lidar, a radar and a radiometer, which allow us to collect and compare data continuously. This method is based on a standardised data format from Cloudnet and can be implemented at any observatory where the Cloudnet data set is available. Two example case studies were chosen from the Atmospheric Radiation Measurement (ARM) Program deployment on Graciosa Island, Azores, Portugal, in 2009 to present the method. We use the cloud droplet effective radius (r_e) to represent cloud microphysical properties and an integrated value of the attenuated backscatter coefficient (ATB) below the cloud to represent the aerosol concentration. All data from each case study are divided into bins of the liquid water path (LWP), each $10\,\mathrm{g\,m^{-2}}$ wide. For every LWP bin we present the correlation coefficient between $\ln r_e$ and $\ln\mathrm{ATB}$, as well as $\mathrm{ACI_r}$ (defined as $\mathrm{ACI_r} = -\mathrm{d}\ln r_e / \mathrm{d}\ln\mathrm{ATB}$, change in cloud droplet effective radius with aerosol concentration). Obtained values of $\mathrm{ACI_r}$ are in the range 0.01–0.1. We show that ground-based remote sensing instruments used in synergy can efficiently and continuously monitor aerosol–cloud interactions.

1 Introduction

The interactions of low-level liquid water clouds with aerosol are considered one of the main sources of uncertainty in climate change predictions. According to the Fifth Assessment Report (AR5) of the Intergovernmental Panel on Climate Change (IPCC, 2014), clouds and the effects of aerosol on their macro- and microstructure continue to contribute to the largest uncertainty in the estimation and interpretation of the Earth's energy budget. Low-level liquid water clouds mainly impact the short-wave radiation budget, as it is mostly sensitive to the cloud albedo. The effect of aerosol concentration on cloud reflectance is often referred to as the albedo effect (Twomey, 1974). The albedo effect is based on the close relation between the aerosol concentration and the cloud droplet concentration.

An ample number of studies have been made to quantify the impact of aerosol concentration on cloud microphysical properties. Studies focusing on low-level liquid water clouds are often based on different methods and instruments. Because of this, the temporal and spatial resolution vary significantly. Observational studies of the aerosol effect on clouds use surface remote sensing instruments at specific locations (e.g. Feingold et al., 2003; Schmidt et al., 2014) or rely on a combination of both surface remote sensing and aircraft in situ observations (e.g. Garrett et al., 2004; Kim et al., 2008; McComiskey et al., 2009). To characterise the aerosol effect on a global scale, many research studies focus on the satellite remote sensing observations (e.g. Kaufman et al., 2005). McComiskey and Feingold (2012) summarised the broad scope of different methods and scales used. They concluded that a single measure of aerosol–cloud interactions (ACIs) used in climate model estimates of the radiative forcing yields widely fluctuating results. ACI is a single measure derived from observational data from varying scales and different assemblies of instruments. Further, they concluded that $\mathrm{ACI_r}$ (defined as $\mathrm{ACI_r} = -\mathrm{d}\ln r_e / \mathrm{d}\ln\alpha$, change in cloud droplet

effective radius with aerosol concentration) is only useful in small-scale measurements. That way it can be measured at a scale of the process it represents, that is, at a microphysical scale. Microphysical changes in cloud and aerosol can be captured by either in situ measurements or point-based remote sensing observations from the ground with a high temporal resolution. Therefore in this paper we focus on a new methodology that allows ACI to be continuously observed with ground-based remote sensing instruments over multiple locations.

We present an approach for monitoring aerosol–cloud interactions with ground-based remote sensing instruments. We use specifically a zenith-pointing cloud radar, a lidar and a microwave radiometer to characterise cloud microphysical properties and the aerosol concentration in the same column. Thanks to the unique capabilities of the ground-based remote sensors, data can be collected and compared continuously. Due to the fine height and time resolution available, cloud and aerosol properties are observed in the same air column. We developed the monitoring scheme on the basis of the standardised data format from Cloudnet (Illingworth et al., 2007). The method described here can be implemented on multiple ground-based observational sites (e.g. the European ACTRIS network – Aerosol, Clouds and Trace gases Research InfraStructure and the US Atmospheric Radiation Measurement (ARM) Program – both databases provide the Cloudnet data set), where a long-term database of measurements already exists. This will allow statistical calculations of ACI to be performed for different locations.

The structure of this paper is as follows: first, we provide a description of the methodology for estimating the relationship between the aerosol concentration below the cloud base and the cloud droplet concentration and the droplet sizes in the cloud base region. We describe the combination of instruments and proxies used in the method. Then we show two example case studies from the ARM Mobile Facility on Graciosa Island, the Azores, Portugal. Finally, we discuss the possibilities of implementing this method over the network of cloud profiling observatories in Europe.

2 Quantifying interactions between aerosol and cloud

Very often in the literature, the term "aerosol–cloud interactions" is associated with the quantification of the impact of aerosol on cloud albedo. This relation was first postulated by Twomey (1974). Through experimental studies he showed that the number concentration of aerosol (N_a) below the cloud is monotonically related to the cloud droplet number concentration (N_d) (Twomey and Warner, 1967):

$$N_d \propto N_a^\gamma, \tag{1}$$

where γ is the proportionality factor. The value of γ varies between 0.7 and 0.8 in different experimental studies (Pruppacher and Klett, 2010; Twomey, 1974), and the theoretical

bounds are between 0 and 1. N_a and N_d are not directly proportional. The increase in the concentration of aerosol that can be activated into cloud droplets can lead to the lowering of the maximum relative humidity in the cloud base region (Twomey, 1974). Twomey (1977) further derived a theoretical relationship between the aerosol concentration and cloud albedo. He proposed that an increased aerosol concentration will lead to an increased cloud droplet concentration and a smaller effective radius of cloud droplets (r_e). A smaller effective radius of cloud droplets will result in a brighter cloud and an increased cloud albedo. This is only true if the amount of available water, represented by the liquid water path (LWP), is constant.

The cloud optical thickness (τ_d) is a function of both the cloud droplet concentration and cloud effective radius. Thus, we can assume that the optical thickness will rise with the increase of the droplet concentration (Twomey, 1974),

$$\tau_d \propto N_d^{1/3}, \tag{2}$$

and the decrease of the droplet radius (Stephens, 1978),

$$\tau_d \propto \frac{\text{LWP}}{r_e}. \tag{3}$$

Theoretical relationships between variables in Eqs. (1), (2) and (3) led to the formulation of a relation between the aerosol optical thickness (τ_a), as τ_a is a function of the aerosol number concentration (N_a), and the effective radius of cloud droplets (r_e) (Feingold, 2003):

$$r_e \propto \tau_a^{-\gamma/3}, \tag{4}$$

which is a basic theoretical relation used presently to quantify the effect described by Twomey (1974). In order to empirically quantify the aerosol–cloud interactions, Feingold et al. (2001) introduced the indirect effect index (IE), later referred to as ACI (aerosol–cloud interactions):

$$IE = ACI_r = -\left. \frac{d\ln r_e}{d\ln\alpha} \right|_{\text{LWP}} \quad 0 < ACI_r < 0.33, \tag{5}$$

and

$$IE = ACI_\tau = \left. \frac{d\ln \tau_d}{d\ln\alpha} \right|_{\text{LWP}} \quad 0 < ACI_\tau < 0.33, \tag{6}$$

or

$$IE = ACI_N = \frac{d\ln N_d}{d\ln\alpha} \quad 0 < ACI_N < 1, \tag{7}$$

where α is an observed proxy of the aerosol concentration. Parameters such as aerosol number concentration (N_a), aerosol optical thickness (τ_a) or aerosol index, which is a product of τ_a and Angström exponent, were used to represent the aerosol concentration in different studies. Note that ACI_N is not bounded by the value of LWP and is derived directly from Eq. (1).

In mathematical terms, ACI_r, ACI_τ and ACI_N are represented by a slope of a linear regression between a logarithm of a cloud property (dependent variable) and a logarithm of an aerosol property (independent variable). Thus, we can write ACI_r as

$$ACI_r = R_{aerosol,cloud} \frac{S_{cloud}}{S_{aerosol}}, \qquad (8)$$

where $R_{aerosol,cloud}$ is the Pearson product-moment correlation coefficient between the logarithm of aerosol property and the logarithm of the cloud property, S_{cloud} is the standard deviation of the cloud property and $S_{aerosol}$ is the logarithm of the aerosol property (McComiskey and Feingold, 2012).

It is important to note that in order to derive Eq. (2) a series of assumptions was made. Twomey and Warner (1967) assumed that cloud is homogeneous. It allowed them to apply properties of the cloud base area to the whole cloud. For a cloud in an early formation stage the cloud droplet concentration is decided mainly by the number of cloud condensation nuclei (CCN) in the cloud base area. By assuming that cloud is homogeneous, the same is true for the whole cloud. Further, Twomey assumed that both cloud droplet number concentration and aerosol optical thickness are directly proportional to an increasing aerosol concentration. This means that he considered all components in the aerosol to increase together and at the same proportion. The combination of these assumptions greatly minimises the number of observational case studies where the relation from Eq. (2) can be applied.

Another important and often omitted factor is that the cloud droplet concentration (N_d) is modified by mixing, collision, coalescence and evaporation within the cloud. However, at the area close to the cloud base, where the cloud is at the early formation stage, the initial N_d is determined by the number of nuclei able to activate into cloud droplets at or below the maximum supersaturation in the cloudy air (Twomey and Warner, 1967). This means that the aerosol concentration should be related to the number concentration of cloud droplets in the cloud base area in observational studies, as translation of this relationship to the whole clouds requires the assumption that cloud is homogeneous – and that is rarely the case.

In this study we focus on the aerosol–cloud interactions as an approximation of the nucleation process without relating them to the cloud albedo. We design a method that enables daily monitoring of the microphysical processes between aerosol and clouds. We quantify the relation between cloud and aerosol properties with statistical parameters. We assume that the aerosol concentration below the cloud is monotonically related to the cloud droplet concentration in the cloud base region (Eq. 1) and that the increase of the cloud droplet concentration leads to a decrease of the cloud droplet size. We perform a logarithmic transformation of both aerosol and cloud properties. Thus, the quantities we use for determining the relation between aerosol concentration and cloud droplet size are the natural logarithm of the attenuated backscatter coefficient (ln ATB) and the natural logarithm of the cloud droplet effective radius ($\ln r_e$) – see Sect. 2.1. We use the Pearson product-moment correlation coefficient, R, to establish how dependent the cloud droplet size is on the aerosol concentration. The sign of the correlation coefficient will show if the increasing concentration of aerosol actually decreases with the cloud droplet size. We further calculate ACI_r (Eq. 5), which as we mentioned before represents the slope of the regression line between the cloud droplet effective radius (r_e) and the aerosol concentration. ACI_r is important to estimate the proportionality factor γ as defined in Eqs. (1) and (4). We also calculate the coefficient of determination, r^2, which suggests the percentage of the variability in cloud droplet size that can be explained by changes in aerosol concentration. We want to analyse data daily when the specific conditions are present (see Sect. 3.2) and divide data into small bins of liquid water path (LWP) to approximate the conditions in each bin to a constant LWP, as postulated by Twomey (1977).

2.1 Aerosol and cloud properties' proxies

Clouds are formed when aerosol particles are activated into cloud droplets. Activation is a change from stable to unstable growth due to the increase of the ambient humidity. When haze droplets reach a critical radius (Köhler, 1936), they are transformed into cloud droplets. When a higher concentration of the aerosol particles is present, the competition for the excess water vapour will be greater and thus, the resulting cloud droplets will be smaller (Lamb and Verlinde, 2011).

In low-level liquid water clouds, in particular stratocumulus, the number of the activated droplets approaches the concentration of the aerosol accumulation mode (particles between 0.1 and 1 μm), making that concentration itself the primary determinant of the cloud droplet concentration (e.g. Martin et al., 1994; Lu et al., 2007). Based on an adiabatic cloud parcel model representing the hygroscopic growth of CCN and droplet condensation, Feingold (2003) concluded that aerosol number concentration (N_a) contributes most significantly to aerosol effects on clouds. Other aerosol parameters, such as size, breadth of the aerosol size distribution and its chemical composition, are of a secondary importance.

2.2 Relation between aerosol and cloud proxies

The strong relation between aerosol concentration and cloud droplet concentration (Eq. 1) is postulated both by theory and observations. We expect to see an inverse relationship between the aerosol concentration and cloud droplets' size. With the increase of the aerosol concentration, the cloud droplet size is expected to decrease, while at the same time, the cloud droplet concentration is expected to increase. This is true if the amount of available water, LWP, is kept constant.

3 Methodology

3.1 Instrumentation and data set

Very often, collocated measurements of aerosol and cloud properties are not available at a similar time resolution. Alternatively, data are only being collected during specific measurements campaigns. This does not allow for a continuous monitoring of aerosol–cloud interactions. To gain a better understanding of the aerosol impact on cloud microphysical properties, we need to have continuous measurements, in different meteorological conditions and over multiple locations. Also, to eliminate rapid variation in the meteorological conditions, we want to evaluate data daily. Ground-based remote sensing instruments are able to provide continuous measurements. They can provide measurements of fine temporal and height resolution that can be used to monitor aerosol–cloud interactions. The goal of our method is to monitor the interactions between aerosol and clouds. We combine measurements from three separate instruments: a cloud radar, a lidar and a microwave radiometer. This combination of instruments can capture and monitor the influence of a changing aerosol concentration on the cloud microphysical properties.

We used the Cloudnet data set, which provides a set of high-quality measurements from a radar, a lidar and a microwave radiometer. The specification of all three instruments may vary slightly per Cloudnet site, but the retrieval algorithms are always the same. The detailed specification of instruments used in this study is presented in Sect. 4. Additionally, each pixel of the time–height grid of the Cloudnet data set is categorised in terms of the presence of liquid droplets (cloud, rain or drizzle), ice, insects or aerosol. This categorisation is a specific product of the Cloudnet data set (Hogan and O'Connor, 2004) and was designed to facilitate the retrieval of cloud microphysical properties. This categorisation product allows us to construct an algorithm that can be applied to specific targets only, liquid water cloud droplets and aerosol, and provides an easy way of selecting data based on a set of selection criteria (Sect. 3.2).

3.1.1 Aerosol number concentration

Numerous proxies have been used in the past to represent the aerosol concentration. In this method we aim to use continuous measurements with a high spatial and temporal resolution. Such a data set is available from a lidar, in the setup of this research, specifically a Vaisala CT25K ceilometer operating at 905 nm. Several research studies indicate that a ceilometer can be used as a quantitative aerosol measurement instrument (Sundström et al., 2009; Wiegner et al., 2014). Backscatter from ceilometers (β) can be approximated to

$$\beta \approx \int_{0}^{\infty} N_{a}(D_{a}) D_{a}^{2} \mathrm{d}D_{a}, \tag{9}$$

where N_a is the number concentration of aerosol and D_a is the aerosol diameter. The averaged β shows good correlation with the in situ measurements of the mass concentration of the particulate matter up to 10 μm (PM10) and smaller than 2.5 μm (PM2.5) (Münkel et al., 2006).

In this method we use a column-integrated value of the attenuated backscatter coefficient (ATB) in order to represent the whole column of aerosol below the cloud. We only consider well-mixed conditions (Sect. 3.2). Specifically, we only look into single-layer clouds on top of the boundary layer with the cloud base below 2000 m. Data are integrated from the level of a complete overlap (minimum height where the cross section of the lidar laser beam is completely in the field of view of the receiver's telescope; Kovalev, 2015), which is 120 m in our study, up to 300 m below the cloud base. The distance from the cloud minimises the amount of cloud and haze droplets or wet aerosol mixed through the considered aerosol background. The specific distance of 300 m was used in other studies based on ground-based lidar measurements (Schmidt et al., 2015).

Very often, a set height of the aerosol concentration proxy is used in the studies of aerosol–cloud interaction (e.g. Raman lidar extinction at 350 m; Feingold et al., 2006). We compared an aerosol property (ATB) and a cloud property (cloud droplet effective radius – r_e) at a set height, 350 m from the ground for the ATB, and a mean value of r_e through the cloud, with the ATB and r_e set at a specific distance from the cloud base (and the cloud base height is seldom constant), 300 m below the cloud for ATB and 85 m above the cloud base for r_e. We found that by considering the level of aerosol proxy (ATB) and cloud proxy (r_e) at a set distance from the cloud base, the dependence of cloud properties on aerosol concentration is bigger. Explicitly, the correlation coefficient, R, has a higher absolute value. Therefore we use a height based on a set distance from the cloud base for both aerosol and cloud properties in this study.

Note that Cloudnet ceilometers are calibrated in accordance with the O'Connor et al. (2004) method which introduces a calibration uncertainty of up to 10 %. The precision of the measurements is difficult to estimate as the internal processing algorithms are proprietary. A single value of 0.5 dB is used for all pixels (Hogan and O'Connor, 2004).

3.1.2 Cloud droplet size and number concentration

Aerosol–cloud interactions are described as the response of the microphysical properties of the cloud to the change of the aerosol concentration. The cloud properties that we are specifically interested in are the cloud droplet size and the number concentration of the droplets. Both these variables are obtained through a retrieval of cloud microphysical properties from measurements.

We apply a method according to Frisch et al. (2002) to retrieve the cloud droplet concentration (N_d) and the cloud droplet effective radius (r_e). This retrieval method uses ob-

servations from a cloud radar and a microwave radiometer (MWR). Assuming that N_d and a gamma cloud droplet distribution, with a fixed distribution shape (ν), are constant with height, the r_e can be derived from the radar reflectivity factor (Z) and the MWR-retrieved LWP:

$$r_e(h) = \left(\frac{(\nu+2)^3}{(\nu+3)(\nu+4)(\nu+5)} \right)^{\frac{1}{3}} \tag{10}$$

$$\times \left(\frac{\pi \rho_w \sum_{i=1}^{n} Z^{\frac{1}{2}}(h_i) \Delta h}{48 \mathrm{LWP}} \right)^{\frac{1}{3}} Z^{\frac{1}{6}}(h),$$

where ρ_w is the density of liquid water (10^6 g m^{-3}), Δh is the length of the radar range gate, $Z(h_i)$ is the reflectivity factor at the ith radar measured gate and n represents the number of the in-cloud radar-measured gates. The cloud droplet number concentration (N_d) is calculated from the following formula:

$$N_d = \left(\frac{(\nu+3)(\nu+4)(\nu+5)}{\nu(\nu+1)(\nu+2)} \right) \tag{11}$$

$$\times \left(\frac{6 \mathrm{LWP}}{\pi \rho_w \sum_{i=1}^{n} Z^{\frac{1}{2}}(h_i) \Delta h} \right).$$

Both of these retrieved properties have been evaluated against other methods in Knist (2014). The comparison of different retrieved microphysical cloud properties revealed that r_e is the parameter least affected by the instrumental errors of the MWR and radar. The estimated uncertainties in r_e are about 10–15 % and in N_d around 40–60 %. In both proxies the uncertainties are due to instrument errors and algorithm assumptions. The main algorithm assumptions include the following: (1) the droplet size distribution is approximated by a mono-modal gamma distribution, (2) the moments of the droplet size distribution are correlated among each other and (3) the droplet concentration and droplet size distribution shape parameter remain constant with height in each profile.

Following Knist (2014), the gamma cloud droplet distribution shape parameter is set to 8.7. This value is obtained from the ratio between the third and second moments of the droplet distribution and has been found in reanalysis of the in situ observations of stratocumulus clouds (Brenguier et al., 2011).

Similarly to the aerosol proxy, we compare the r_e at a set distance from the cloud base. We set this distance at 85 m above the cloud base detected from the lidar measurements. Lidar can detect the cloud base height more precisely than radar; the difference can be up to two range gates. Hence we use the distance of 85 m, which is equal to two range gates, to ensure that the cloud is detected by both instruments.

3.2 Data selection criteria

Clouds are complicated systems with many processes taking place at the same time. Singling out a small microphys-

ical process is difficult. Data need to be limited by implementing a number of filters. Firstly, this monitoring scheme applies only to liquid water clouds on top of the boundary layer in well-mixed conditions, where the cloud base is located below 2000 m. This limitation ensures that the cloud is not decoupled from the boundary layer and the aerosol background below the cloud (Feingold et al., 2006). Secondly, we can only consider data where no precipitation is present, including drizzle, as it can obscure the formative stage of a cloud (Feingold et al., 2003). We use the Cloudnet categorisation data for the classification of the observed targets. This scheme relies on the measurements from three separate instruments. Only profiles where all three instruments provide good-quality data can be analysed. Data quality is classified in the Cloudnet data set in a similar way to the categorisation product. We can therefore easily filter data where a problem with the measurements was detected.

Some larger scale factors, such as boundary layer dynamics or variations in temperature, pressure or humidity, can influence changes in the cloud. We ensure similar meteorological conditions by analysing aerosol and cloud properties on a daily basis. This minimises the influence of variations in general weather conditions. However, the transition between meteorological conditions can happen within a day and often even at a smaller timescale. To account for these kinds of daily changes, we use filters of the meteorological conditions, namely temperature, pressure and specific humidity. For each parameter we calculate a mean value and a standard deviation; if the standard deviation is below 10 % of the mean value, we consider that as similar meteorological conditions. We use the integrated value of ATB as a proxy of aerosol concentration. As we mentioned before, we integrate ATB in the column from 120 m above the ground (level of complete overlap) to 300 m below the cloud base height. This limits the possible cloud base height to above 500 m above ground level, if the ATB is to be integrated over at least two ranges.

We also apply a constraint on LWP to isolate the aerosol activation process from different interactions that can happen at the same time. Daily data sets are divided into profiles where the value of LWP is similar. We divide the data into bins of LWP of 10 g m^{-2}. Creating even smaller bins is difficult due to the limited data points. We only consider LWP bins where the total number of data points is above 20. LWP should be above 30 g m^{-2} and below 150 g m^{-2}. Values below 30 g m^{-2} are disregarded because of the uncertainty of LWP calculated from the MWR, which is around 15 g m^{-2} (Turner et al., 2007). The values above 150 g m^{-2} are excluded to avoid precipitating clouds.

The analysis of an aggregated data set grouped by varying meteorological conditions (as defined above) would be a good way of getting a better understanding of the drivers of aerosol–cloud interactions. Such a study can be carried out using the monitoring method presented in this study, but is beyond the scope of this paper.

Table 1. Cloud and aerosol properties measured or derived from the observations at the Graciosa Island, Azores.

Measured quantity	Definition	Instrument(s)
Cloud liquid water path	LWP ($g\,m^{-2}$)	MWR
Radar reflectivity factor	Z (dBZ or $m^6\,m^{-3}$)	WACR
Cloud droplet effective radius	r_e (µm) (see Eq. 10)	WACR/MWR
Cloud droplets number concentration	N_d (cm^{-3}) (see Eq. 11)	WACR/MWR
Attenuated backscatter coefficient	ATB ($m^{-1}\,sr^{-1}$)	Vaisala CT25K

4 Application of the method to observations from Graciosa Island, Azores

We present here two example case studies of the practical application. The deployment of the Atmospheric Radiation Measurement (ARM) Program Mobile Facility on Graciosa Island, Azores, in 2009 and 2010 provides a comprehensive data set for assessing aerosol effects on low-level liquid water clouds. Boundary-layer clouds were the most frequently observed cloud type (40–50 %), with the maximum occurrence during the summer and autumn months under the presence of anticyclonic conditions (Rémillard et al., 2012). The instruments we use in this study are a W-band ARM Cloud Radar (WACR) operating at 95 GHz (Widener, 2004), a laser ceilometer Vaisala CT25K operating at 905 nm and a two-channel microwave radiometer (MWR) operating at 23 and 31.4 GHz. Data from this campaign are available in the standardised Cloudnet format, which is the basis of calculations presented here. The Cloudnet data set is re-gridded to the vertical resolution of the radar (42.86 m) and the time resolution of the radiometer (30 s). Table 1 summarises all measurements and all products derived for the data analysis.

Based on the data selection criteria presented in the section above, we identified two case studies for testing the method: 3 and 29 November 2009. Both cases showed only a small variability of the LWP which enabled distribution of data into small bins of LWP $g\,m^{-2}$. The station was located at the north-east shore of the island, situated upwind in order to reduce the impact of the island. The NOAA HYSPLIT back trajectory model (National Oceanic and Atmospheric Administration Hybrid Single Particle Lagrangian Integrated Trajectory Model Draxler et al., 1997) indicated that the aerosol for the selected days came from marine sources. This single source of aerosol allowed us to test the method without adding the extra complexity of a multiple aerosol sources background. We chose two case studies from the same season, with similar meteorological conditions. Cases vary in the cloud base height and in the aerosol loading.

4.1 Study case from 3 November 2009

The conditions on 3 November 2009 were characterised by a northerly wind of about 2.5 m s^{-1} in the boundary layer. The cloud cover persisted the whole day, with periods of drizzle and heavy rain after 18:00 UTC. Precipitation-free periods
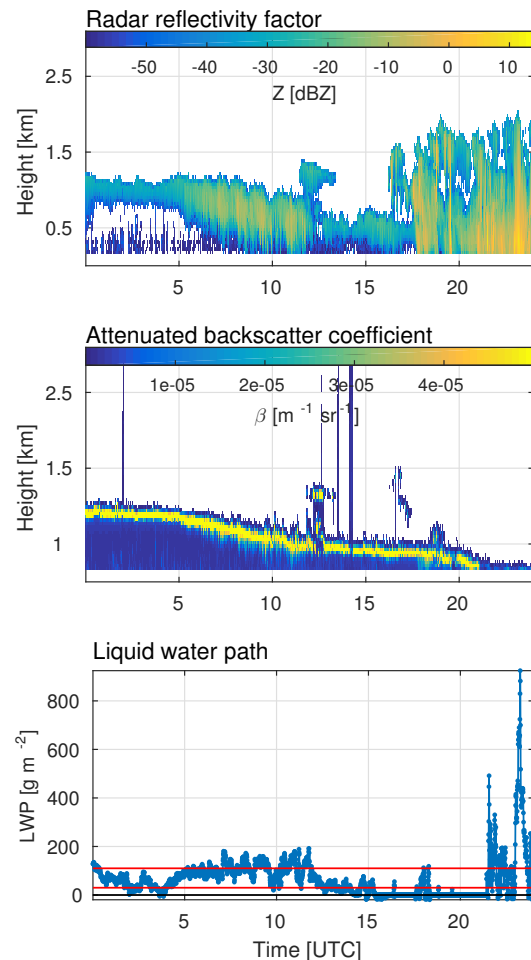

Figure 1. The time–height cross section of the radar reflectivity factor from WACR, the attenuated backscatter coefficient from Vaisala CT25K and the liquid water path from the MWR for a full day of measurements on 3 November 2009.

were identified between 00:00 and 05:00 UTC, with a second short period between 13:30 and 15:00 UTC, after a light precipitation event (Fig. 1). Based on the Cloudnet categorisation and the measurements from WACR and the MWR, only data in these two periods were analysed on that day. LWPs in the selected periods ranged from 15 to 130 $g\,m^{-2}$. As few data points were available with an LWP above 90 $g\,m^{-2}$, we limit the data analysed to an LWP between
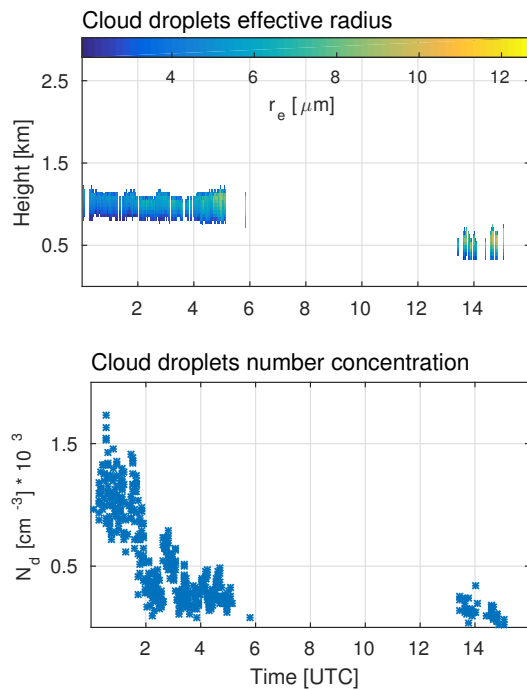
Figure 2. The time–height cross section of the cloud droplet effective radius (r_e) calculated from WACR and MWR measurements (Eq. 10) and the cloud droplet number concentration (N_d) calculated from Eq. (11) from 3 November 2009. Data are only retrieved in the time steps when the data selection criteria are met.

Figure 3. The time–height cross section of the radar reflectivity from WACR, the attenuated backscatter coefficient from Vaisala CT25K and the liquid water path from the MWR for a full day of measurements on 29 November 2009.

30 and 90 g m^{-2}. The cloud base was located around 800 m above ground level (a.g.l.) between 00:00 and 05:00 UTC and around 500 m a.g.l. between 13:30 and 15:00 UTC.

Figure 2 presents the time–height cross section of the retrieved microphysical cloud properties. Only data from time steps meeting the data selection criteria are calculated. In the chosen periods, r_e varies from 3 to 7 µm, with a mean radius of 5 µm and a standard deviation of 0.75 µm. N_d ranges in the selected periods from 150 to 1700 cm^{-3}. Some values are much higher than the observational data for stratocumulus. N_d rarely exceeds 500 cm^{-3} and is generally lower (200–300 cm^{-3}) for marine stratocumulus (Martin et al., 1994).

Aerosol background (represented by ATB) in the selected periods is variable with the mean value 0.64 × 10^{-3} sr^{-1} and a standard deviation of 0.18 × 10^{-3} sr^{-1}. ATB in the period between 13:30 and 15:00 UTC is significantly lower, mainly because it was followed by a period of precipitation and the cloud base was located considerably lower than in the first period.

All data points available on 3 November 2009 are divided into bins based on the value of the LWP which ranges from 30 to 90 g m^{-2}. Data were divided into six separate bins, each covering 10 g m^{-2}. Figure 5 presents the relation between the integrated attenuated backscatter ATB and cloud droplet effective radius r_e. The calculated values of the correlation co-
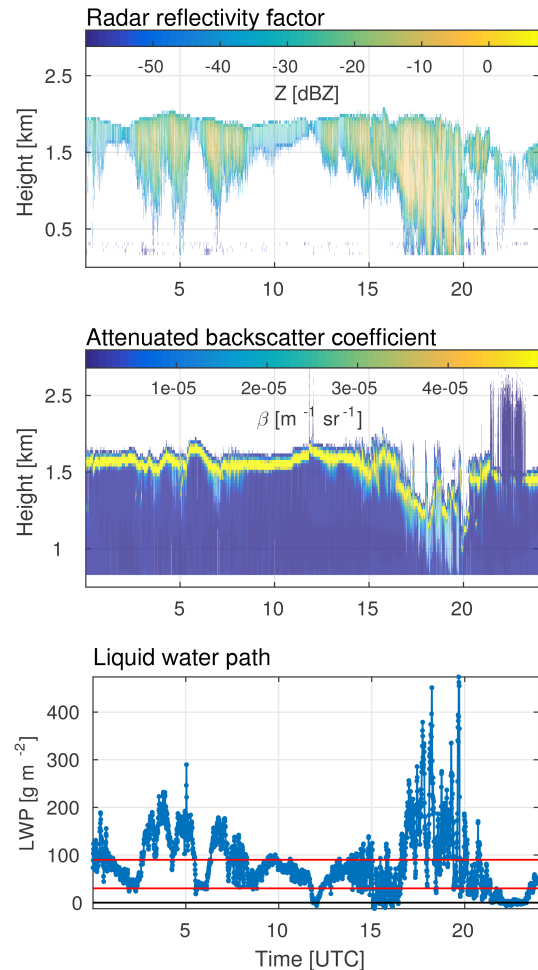
efficient, R, and ACI$_r$ are presented for every bin. Both R and ACI$_r$ are calculated for the ln ATB and ln r_e (Eq. 5).

Table 2 summarises values of R, ACI$_r$ and the coefficient of determination, r^2, for every LWP bin. The coefficient of determination, r^2, suggests the percentage of the variability in cloud droplet size that can be explained by changes in aerosol concentrations. Note that both R and ACI$_r$ values are highest for 3 November 2009 in the LWP range from 40 to 70 g m^{-2}. This may indicate that aerosol–cloud interactions representing the activation process are more significant only for the lower LWP values, and for the higher values of LWP, other processes, such as collision and coalescence of cloud droplets or cloud top cooling, may play a more important role. Another possible explanation can be the presence of drizzle when LWP is above 70 g m^{-2}. Some studies suggest that marine stratocumulus clouds can form drizzle particles at LWP values as low as 75–100 g m^{-2} (Rémillard et al., 2012).

Table 2. ACI$_r$ (Eq. 5) and the statistical parameters calculated between $\ln(r_e)$ and $\ln(\text{ATB})$, namely Pearson product-moment correlation coefficient, R, and the coefficient of determination, r^2, and the number of observations within the LWP bins, n, for two case studies from Graciosa Island, the Azores (3 and 29 November 2009).

	3 November 2009				29 November 2009			
LWP bin	ACI$_R$	R	r^2	n	ACI$_r$	R	r^2	n
$30 < \text{LWP} < 40$	0.01	−0.09	0.01	63	0.08	−0.50	0.25	45
$40 < \text{LWP} < 50$	0.06	−0.36	0.13	34	0.08	−0.52	0.27	63
$50 < \text{LWP} < 60$	0.06	−0.41	0.16	49	0.07	−0.56	0.31	67
$60 < \text{LWP} < 70$	0.04	−0.30	0.09	92	0.09	−0.65	0.42	96
$70 < \text{LWP} < 80$	0.00	−0.03	0.00	50	0.05	−0.39	0.16	98
$80 < \text{LWP} < 90$	0.08	−0.26	0.07	32	0.03	−0.27	0.07	39

Figure 7 shows the relation between the integrated attenuated backscatter, ATB, and the cloud droplet number concentration, N_d, together with the corresponding R and ACI$_N$ (Eq. 7). Cloud droplet number concentration increases with the increase of aerosol concentration (represented by ATB) as expected by the aerosol–cloud interactions. Table 3 summarises values of R, ACI$_N$ and the coefficient of determination, r^2, for both study cases.

4.2 Study case from 29 November 2009

On 29 November 2009 a northerly wind of about $2\,\text{m s}^{-1}$ in the boundary layer persisted most of the day. Periods of drizzle and rain occurred throughout the day, with heavy precipitation after 15:00 UTC. Therefore we only consider data before 15:00 UTC.

The cloud base was located around 1600 m a.g.l. (Fig. 3). Periods between 00:00 and 03:00, 05:30 and 06:00 and 08:30 and 14:00 UTC correspond with the data selection criteria. In all cases, the categorisation provided by Cloudnet identifies that the cloud layer consists of liquid water cloud and aerosol only. LWP in the selected periods varies between 15 and $150\,\text{g m}^{-2}$. As there are few data points available with an LWP above $90\,\text{g m}^{-2}$, we limit the data analysed to an LWP between 30 and $90\,\text{g m}^{-2}$.

Figure 4 shows the retrieved properties in periods corresponding to our data selection criteria. In the selected periods N_d varies from 55 to $1900\,\text{cm}^{-3}$, with a standard deviation of $380\,\text{cm}^{-3}$ and mean value of $750\,\text{cm}^{-3}$. Values of r_e range between 2.5 and $7\,\mu\text{m}$, with a mean radius $4.6\,\mu\text{m}$ and a standard deviation of $0.65\,\mu\text{m}$. ATB in the selected period has a mean value of $1.53 \times 10^{-3}\,\text{sr}^{-1}$ and a standard deviation of $0.25 \times 10^{-3}\,\text{sr}^{-1}$. It should be noted that on 29 November, ATB is higher, but, even accounting for the uncertainty of ATB, the variation is smaller than on 3 November.

Suitable data from 29 November 2009 are divided into bins based on the value of the LWP which ranges from 30 to $90\,\text{g m}^{-2}$. Data were divided into six separate bins, each covering $10\,\text{g m}^{-2}$. Figure 6 presents the relation between the integrated attenuated backscatter, ATB, and cloud droplet ef-
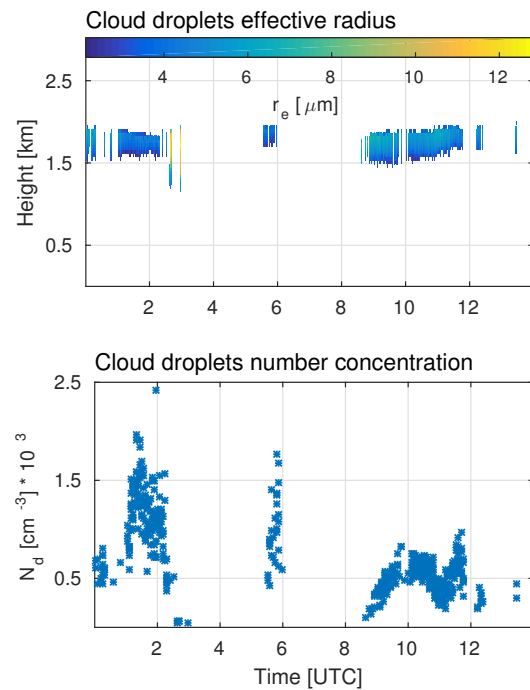

Figure 4. The time–height cross section of the cloud droplet effective radius (r_e) derived from the WACR and the MWR (Eq. 10) and the cloud droplet number concentration (N_d) calculated from Eq. (11) from 29 November 2009. Data are only retrieved in the time steps when the data selection criteria are met.

fective radius, r_e, together with the correlation coefficient, R, and ACI$_r$ calculated for each bin. It can be observed that data points are less scattered on the 29 November than on the 3 November, and the values of both R and ACI$_r$ are also higher. Similar to the case from the 3 November, R and ACI$_r$ are highest in the LWP range between 40 and $70\,\text{g m}^{-2}$.

Figure 8 presents the relation between the integrated attenuated backscatter, ATB, and the cloud droplet number concentration, N_d, together with the corresponding R and ACI$_N$.
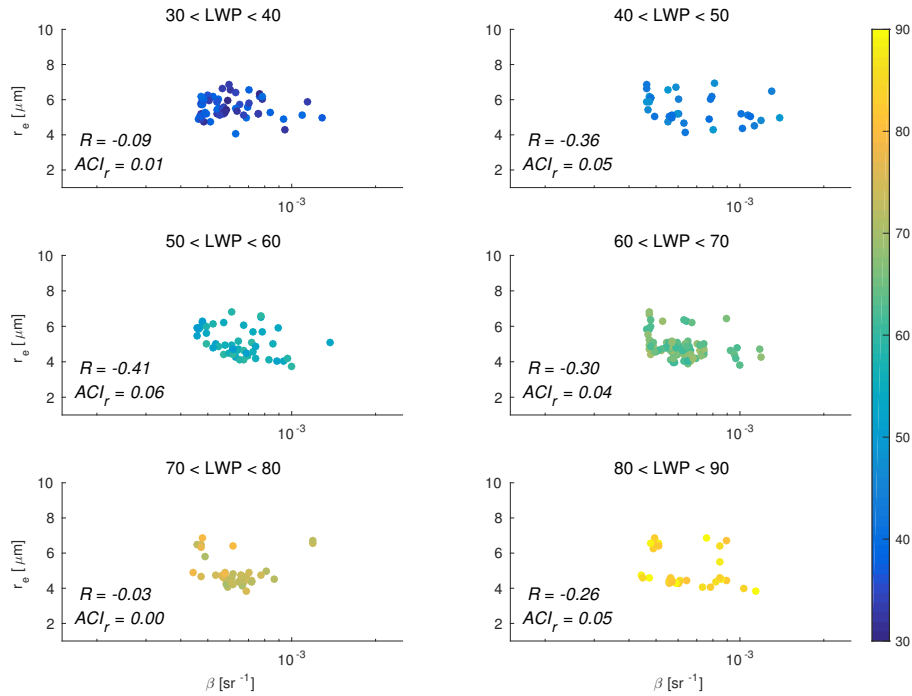
Figure 5. The values of the effective radius, r_e, derived from WACR and MWR measurements are plotted versus the integrated attenuated backscatter ATB measured by Vaisala CT25K on 3 November 2009. Data are sorted by the values of LWP from the MWR. Every panel shows the corresponding value of ACI_r (Eq. 5) and the Pearson product-moment correlation coefficient, R, for that LWP bin.
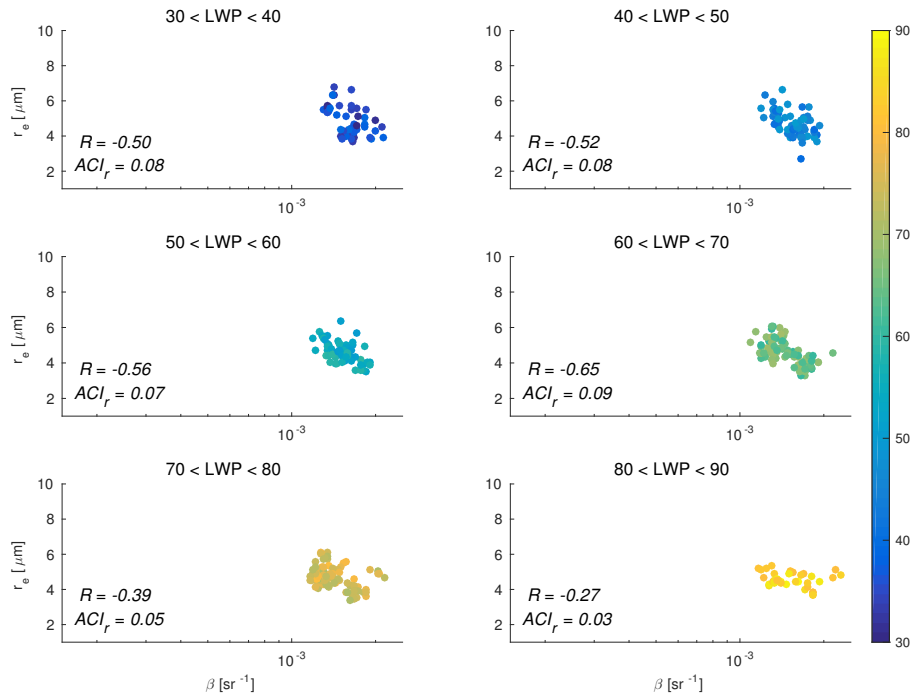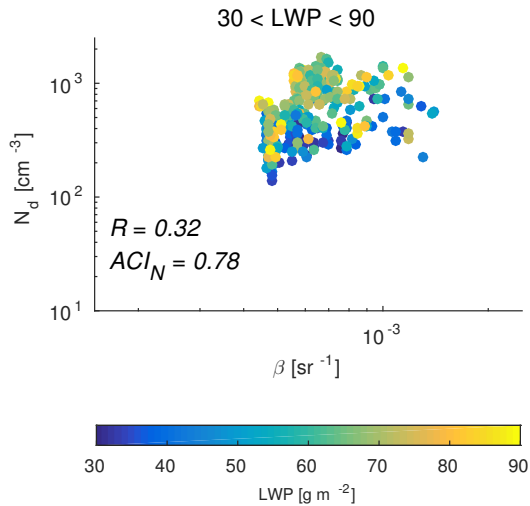

Figure 6. The values of the effective radius, r_e, derived from WACR and MWR measurements are plotted versus the integrated attenuated backscatter ATB measured by Vaisala CT25K on 29 November 2009. Data are sorted by the values of LWP from the MWR. Every panel shows the corresponding value of ACI_r (Eq. 5) and the Pearson product-moment correlation coefficient, R, for that LWP bin.
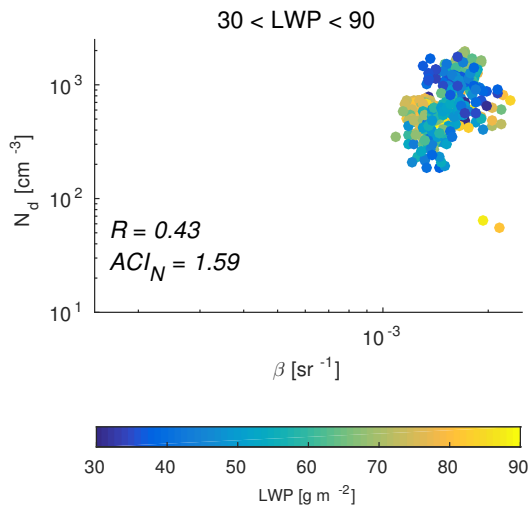
Figure 7. The cloud droplet number concentration, N_{d}, derived from WACR and MWR measurements with Eq. (11) is plotted versus the integrated attenuated backscatter ATB measured by Vaisala CT25K on 3 November 2009. The corresponding value of $\mathrm{ACI_N}$ (Eq. 7) and the Pearson product-moment correlation coefficient, R, is presented.

Figure 8. The cloud droplet number concentration, N_{d}, derived from WACR and MWR measurements with Eq. (11) is plotted versus the integrated attenuated backscatter ATB measured by Vaisala CT25K on 29 November 2009. The corresponding value of $\mathrm{ACI_N}$ (Eq. 7) and the Pearson product-moment correlation coefficient, R, is presented.

4.3 Comparison of example case studies

Table 2 summarises statistical parameters, including the number of observations within each LWP bin, for both case studies presented here. Values of the correlation coefficient, r, are generally higher for the value of LWP in the range from 40 to 70 g m^{-2}. This suggests that aerosol–cloud interactions

Table 3. $\mathrm{ACI_N}$ (Eq. 7) and the statistical parameters calculated between $\ln(N_{\mathrm{d}})$ and $\ln(\mathrm{ATB})$, namely the Pearson product-moment correlation coefficient, R, and the coefficient of determination, r^2, and the number of observations, n, for two case studies from Graciosa Island, the Azores (3 and 29 November 2009).

3 November 2009				29 November 2009			
$\mathrm{ACI_N}$	R	r^2	n	$\mathrm{ACI_N}$	R	r^2	n
0.78	0.32	0.10	320	1.59	0.43	0.19	408

connected to the droplet activation play a more important role in the lower values of LWP, and that supposedly, drizzle can obscure the process of the activation of aerosol into cloud droplets. For both cases the calculated values of $\mathrm{ACI_N}$ are very high, with a value on the 29 November of 1.59, which exceeds the theoretical bounds (from 0 to 1). This is possibly due to an overestimation of the cloud droplet number concentration (N_{d}) by the retrieval. As we mentioned before, the observational values of N_{d} for marine stratocumulus clouds are around 200–300 cm^{-3} and the retrieved values for both case studies presented here exceed this range drastically. Therefore, we think that it is more reasonable to compare the values of $\mathrm{ACI_r}$, which are between 0 and 0.09 in this study. This range of $\mathrm{ACI_r}$ is comparable to other studies of aerosol–cloud interactions performed with ground-based remote sensing instruments (for example, reported values range from 0.04 to 0.15 in McComiskey et al., 2009).

5   Summary and outlook

In this paper we present a method for observing aerosol–cloud interactions. This method enables continuous monitoring of cloud microphysical responses to the changing aerosol concentration. It utilises high-resolution ground-based remote sensing instruments. This scheme is developed on the basis of a standardised data format from Cloudnet. Therefore, this method can be applied at any ground-based cloud observatory participating in the Cloudnet network. We used the Cloudnet cloud categorisation product to choose data points with the specific targets only (liquid water clouds and aerosol). Instead of aggregating data with the same values of LWP over a longer period, we process data from each day separately.

Daily data for analysis are selected based on a range of criteria. Data points complying with all of them are divided into bins of LWP where each bin is 10 g m^{-2} wide. For every bin we calculate the Pearson product-moment correlation coefficient, R, $\mathrm{ACI_r}$ (Eq. 5) and the coefficient of determination, r^2. We show that both the statistical parameters and $\mathrm{ACI_r}$ can be used to quantify the dependence of the cloud droplet size on the aerosol concentration. We showed that it is possible to derive $\mathrm{ACI_r}$ and the statistical parameters on a daily

basis and with that ensure that no large variation in the meteorological conditions is present. Collocation of daily data into larger data sets can be carried out, but should be based on very similar meteorological conditions. In our study we identified similar meteorological conditions based on temperature, pressure and specific humidity. We say that the conditions are similar if the standard deviation of each parameter is less than 10 % of its mean value.

We showed two example case studies to present this method. Both data sets come from the deployment of the Atmospheric Radiation Measurement (ARM) Program Mobile Facility on Graciosa Island, Azores, in 2009 and 2010. The presented cases both are characterised by marine stratocumulus clouds; both occur in November and have similar general meteorological conditions. We show the correlation coefficient, ACI_r, and the coefficient of determination for both cases and all the LWP bins. We observe a higher correlation of aerosol concentration and cloud properties in the lower values of LWP (from 40 to 70 g m^{-2}). This suggests that aerosol–cloud interactions are more significant processes at lower LWPs, and when the LWP increases, other processes such as collision and coalescence are the dominant cloud microphysical processes for the case studies presented here. A study based on a bigger data set should be performed to draw more general conclusions. We also observed an increase of the correlation between the aerosol and cloud properties when the parameters are compared at a set height dependent on the cloud base height.

The method we developed is based on a synergy of widely available, high-resolution ground-based remote sensing instruments. It enables the interactions of aerosol and clouds to be monitored. Although data need to comply with restrictive criteria, the use of a Cloudnet data format and the categorisation product makes data selection possible close to real time. We showed that using the integrated value of the attenuated backscatter from lidar enables the monitoring of aerosol–cloud interactions. The measurements from a radar, a lidar and a microwave radiometer are collected continuously and can therefore provide a continuous estimate of the effects of aerosol concentration on cloud properties. This framework of measurements can be implemented at any observatory where the Cloudnet data set is available and can be integrated into a Cloudnet framework as one of the standard products. The software developed for this methodology is available under the GNU General Public License (Sarna, 2015). Monitoring aerosol–cloud interactions in the same manner over multiple regions will allow for more studies of these phenomena and will result in a better understanding of the interactions between aerosol and clouds.

References

Brenguier, J.-L., Burnet, F., and Geoffroy, O.: Cloud optical thickness and liquid water path – does the k coefficient vary with droplet concentration?, Atmos. Chem. Phys., 11, 9771–9786, doi:10.5194/acp-11-9771-2011, 2011.

Draxler, R. R. and Hess, G. D.: Description of the HYSPLIT-4 Modeling System, National Oceanic and Atmospheric Administration, Silver Spring, MD, USA, 1997.

Feingold, G.: Modeling of the first indirect effect: analysis of measurement requirements, Geophys. Res. Lett., 30, 1997, doi:10.1029/2003GL017967, 2003.

Feingold, G., Remer, L. A., Ramaprasad, J., and Kaufman, Y. J.: Analysis of smoke impact on clouds in Brazilian biomass burning regions: an extension of Twomey's approach, J. Geophys. Res., 106, 22907–22922, doi:10.1029/2001JD000732, 2001.

Feingold, G., Eberhard, W. L., Veron, D. E., and Previdi, M.: First measurements of the Twomey indirect effect using ground-based remote sensors, Geophys. Res. Lett., 30, 1287, doi:10.1029/2002GL016633, 2003.

Feingold, G., Furrer, R., Pilewskie, P., Remer, L. A., Min, Q., and Jonsson, H.: Aerosol indirect effect studies at Southern Great Plains during the May 2003 Intensive Operations Period, J. Geophys. Res., 111, D05S14, doi:10.1029/2004JD005648, 2006.

Frisch, S., Shupe, M., Djalalova, I., Feingold, G., and Poellot, M.: The retrieval of stratus cloud droplet effective radius with cloud radars, J. Atmos. Ocean. Tech., 19, 835–842, doi:10.1175/1520-0426(2002)019<0835:TROSCD>2.0.CO;2, 2002.

Garrett, T. J., Zhao, C., Dong, X., Mace, G. G., and Hobbs, P. V.: Effects of varying aerosol regimes on low-level Arctic stratus, Geophys. Res. Lett., 31, L17105, doi:10.1029/2004GL019928, 2004.

Hogan, R. J. and O'Connor, E. J.: Facilitating cloud radar and lidar algorithms: the Cloudnet Instrument Synergy/Target Categorization product, CLOUDNET Project Documentation, Reading, UK, 2004.

Illingworth, A. J., Hogan, R. J., O'Connor, E. J., Bouniol, D., Delanoë, J., Pelon, J., Protat, A., Brooks, M. E., Gaussiat, N., Wilson, D. R., Donovan, D. P., Baltink, H. K., van Zadelhoff, G.-J., Eastment, J. D., Goddard, J. W. F., Wrench, C. L., Haeffelin, M., Krasnov, O. A., Russchenberg, H. W. J., Piriou, J.-M., Vinit, F., Seifert, A., Tompkins, A. M., and Willén, U.: Cloudnet,

B. Am. Meteorol. Soc., 88, 883–898, doi:10.1175/BAMS-88-6-883, 2007.

IPCC: Climate Change 2013 – The Physical Science Basis: Working Group I Contribution to the Fifth Assessment Report of the Intergovernmental Panel on Climate Change, Cambridge University Press, Cambridge, 2014.

Kaufman, Y. J., Koren, I., Remer, L. A., Rosenfeld, D., and Rudich, Y.: The effect of smoke, dust, and pollution aerosol on shallow cloud development over the Atlantic Ocean, P. Natl. Acad. Sci. USA, 102, 11207–11212, doi:10.1073/pnas.0505191102, 2005.

Kim, B.-G., Miller, M. A., Schwartz, S. E., Liu, Y., and Min, Q.: The role of adiabaticity in the aerosol first indirect effect, J. Geophys. Res., 113, D05210, doi:10.1029/2007JD008961, 2008.

Knist, C. L.: Retrieval of liquid water cloud properties from ground-based remote sensing observations, PhD thesis, TU Delft, Civil Engineering and Geosciences, Geoscience and Remote Sensing, Delft, the Netherlands, 2014.

Kovalev, V. A.: Solutions in LIDAR Profiling of the Atmosphere, John Wiley & Sons, Hoboken, NJ, USA, 2015.

Köhler, H.: The nucleus in and the growth of hygroscopic droplets, T. Faraday Soc., 32, 1152–1161, doi:10.1039/TF9363201152, 1936.

Lamb, D. and Verlinde, J.: Physics and Chemistry of Clouds, Cambridge University Press, Cambridge, UK, 2011.

Lu, M.-L., Conant, W. C., Jonsson, H. H., Varutbangkul, V., Flagan, R. C., and Seinfeld, J. H.: The Marine Stratus/Stratocumulus Experiment (MASE): aerosol–cloud relationships in marine stratocumulus, J. Geophys. Res., 112, D10209, doi:10.1029/2006JD007985, 2007.

Martin, G. M., Johnson, D. W., and Spice, A.: The measurement and parameterization of effective radius of droplets in warm stratocumulus clouds, J. Atmos. Sci., 51, 1823–1842, doi:10.1175/1520-0469(1994)051<1823:TMAPOE>2.0.CO;2, 1994.

McComiskey, A. and Feingold, G.: The scale problem in quantifying aerosol indirect effects, Atmos. Chem. Phys., 12, 1031–1049, doi:10.5194/acp-12-1031-2012, 2012.

McComiskey, A., Feingold, G., Frisch, A. S., Turner, D. D., Miller, M. A., Chiu, J. C., Min, Q., and Ogren, J. A.: An assessment of aerosol–cloud interactions in marine stratus clouds based on surface remote sensing, J. Geophys. Res., 114, D09203, doi:10.1029/2008JD011006, 2009.

Münkel, C., Eresmaa, N., Räsänen, J., and Karppinen, A.: Retrieval of mixing height and dust concentration with lidar ceilometer, Bound.-Lay. Meteorol., 124, 117–128, doi:10.1007/s10546-006-9103-3, 2006.

O'Connor, E. J., Illingworth, A. J., and Hogan, R. J.: A technique for autocalibration of cloud lidar, J. Atmos. Ocean. Tech., 21, 777–786, doi:10.1175/1520-0426(2004)021<0777:ATFAOC>2.0.CO;2, 2004.

Pruppacher, H. R. and Klett, J. D.: Microphysics of Clouds and Precipitation, Springer, Dordrecht, Netherlands, 2010.

Rémillard, J., Kollias, P., Luke, E., and Wood, R.: Marine boundary layer cloud observations in the Azores, J. Climate, 25, 7381–7398, doi:10.1175/JCLI-D-11-00610.1, 2012.

Sarna, K.: ACI monitoring: first release, doi:10.5281/zenodo.32033, Computer Software, 2015.

Schmidt, J., Ansmann, A., Bühl, J., Baars, H., Wandinger, U., Müller, D., and Malinka, A. V.: Dual-FOV Raman and Doppler lidar studies of aerosol-cloud interactions: Simultaneous profiling of aerosols, warm-cloud properties, and vertical wind, J. Geophys. Res.-Atmos., 119, 5512–5527, doi:10.1002/2013JD020424, 2014.

Schmidt, J., Ansmann, A., Bühl, J., and Wandinger, U.: Strong aerosol-cloud interaction in altocumulus during updraft periods: lidar observations over central Europe, Atmos. Chem. Phys., 15, 10687–10700, doi:10.5194/acp-15-10687-2015, 2015.

Stephens, G. L.: Radiation profiles in extended water clouds. II: Parameterization schemes, J. Atmos. Sci., 35, 2123–2132, doi:10.1175/1520-0469(1978)035<2123:RPIEWC>2.0.CO;2, 1978.

Sundström, A.-M., Nousiainen, T., and Petäjä, T.: On the quantitative low-level aerosol measurements using ceilometer-type lidar, J. Atmos. Ocean. Tech., 26, 2340–2352, doi:10.1175/2009JTECHA1252.1, 2009.

Turner, D. D., Vogelmann, A. M., Johnson, K., Miller, M., Austin, R. T., Barnard, J. C., Flynn, C., Long, C., McFarlane, S. A., Cady-Pereira, K., Clough, S. A., Chiu, J. C., Khaiyer, M. M., Liljegren, J., Lin, B., Minnis, P., Marshak, A., Matrosov, S. Y., Min, Q., O'Hirok, W., Wang, Z., and Wiscombe, W.: Thin liquid water clouds: their importance and our challenge, B. Am. Meteorol. Soc., 88, 177–190, doi:10.1175/BAMS-88-2-177, 2007.

Twomey, S.: Pollution and the planetary albedo, Atmos. Environ., 8, 1251–1256, doi:10.1016/0004-6981(74)90004-3, 1974.

Twomey, S.: The influence of pollution on the shortwave albedo of clouds, J. Atmos. Sci., 34, 1149–1152, doi:10.1175/1520-0469(1977)034<1149:TIOPOT>2.0.CO;2, 1977.

Twomey, S. and Warner, J.: Comparison of measurements of cloud droplets and cloud nuclei, J. Atmos. Sci., 24, 702–703, doi:10.1175/1520-0469(1967)024<0702:COMOCD>2.0.CO;2, 1967.

Widener, K. B. and Mead, J. B.: W-Band ARM cloud radar-Specifications and design, in: Fourteenth ARM Science Team Meeting Proceedings, Albuquerque, NM, USA, available at: http://www.arm.gov/publications/proceedings/conf14/extended_abs/widener2-kb.pdf, 2004.

Wiegner, M., Madonna, F., Binietoglou, I., Forkel, R., Gasteiger, J., Geiß, A., Pappalardo, G., Schäfer, K., and Thomas, W.: What is the benefit of ceilometers for aerosol remote sensing? An answer from EARLINET, Atmos. Meas. Tech., 7, 1979–1997, doi:10.5194/amt-7-1979-2014, 2014.